

# Data-analysis software framework 2DMAT and its application to experimental measurements for two-dimensional material structures

Yuichi Motoyama<sup>a</sup>, Kazuyoshi Yoshimi<sup>a</sup>, Izumi Mochizuki<sup>b</sup>, Harumichi Iwamoto<sup>c</sup>, Hayato Ichinose<sup>d</sup>, Takeo Hoshi<sup>c,b,d,e</sup>

<sup>a</sup>Institute for Solid State Physics, University of Tokyo, Kashiwa-shi, Chiba 277-8581 Japan

<sup>b</sup>Slow Positron Facility, Institute of Materials Structure Science, High Energy Accelerator Research Organization (KEK), Oho 1-1, Tsukuba, Ibaraki 305-0801, Japan

<sup>c</sup>Department of Mechanical and Physical Engineering, Faculty of Engineering, Tottori University, Tottori-shi, Tottori 680-8552, Japan

<sup>d</sup>Department of Engineering, Graduate School of Sustainability Science, Tottori University, Tottori-shi, Tottori 680-8552, Japan

<sup>e</sup>Advanced Mechanical and Electronic System Research Center, Faculty of Engineering, Tottori University, Tottori-shi, Tottori 680-8552, Japan

arXiv:2204.04484v2 [cond-mat.mtrl-sci] 12 Jul 2022

## Abstract

An open-source data-analysis framework 2DMAT has been developed for experimental measurements of two-dimensional material structures. 2DMAT offers five analysis methods: (i) Nelder-Mead optimization, (ii) grid search, (iii) Bayesian optimization, (iv) replica exchange Monte Carlo method, and (v) population-annealing Monte Carlo method. Methods (ii) through (v) are implemented by parallel computation, which is efficient not only for personal computers but also for supercomputers. The current version of 2DMAT is applicable to total-reflection high-energy positron diffraction (TRHEPD), surface X-ray diffraction (SXR), and low-energy electron diffraction (LEED) experiments by installing corresponding forward problem solvers that generate diffraction intensity data from a given dataset of the atomic positions. The analysis methods are general and can be applied also to other experiments and problems.

**Keywords:** data analysis for experimental measurements, Nelder-Mead optimization, Bayesian optimization, grid search, replica exchange Monte Carlo method, population-annealing Monte Carlo method, two-dimensional material, total-reflection high-energy positron diffraction, surface X-ray diffraction, low-energy electron diffraction

## PROGRAM SUMMARY

2DMAT– Open-source data-analysis framework for experimental measurement of two-dimensional material structures

**Authors:** Yuichi Motoyama, Kazuyoshi Yoshimi, Izumi Mochizuki, Harumichi Iwamoto, Hayato Ichinose, Takeo Hoshi

**Program title:** 2DMAT

**Journal reference:**

**Catalogue identifier:**

**Program summary URL:**

<https://www.pasums.issp.u-tokyo.ac.jp/2dmat/>

**Licensing provisions:** GNU General Public License v3.0

**Programming language:** Python 3

**Computer:** Any architecture

**Operating system:** Unix, Linux, macOS

**RAM:** Depends on the number of variables

**Number of processors used:** Arbitrary

**Keywords:** Nelder-Mead optimization, Bayesian optimization, grid-based search, replica exchange Monte Carlo method, population-annealing Monte Carlo method, total-reflection high-energy positron diffraction (TRHEPD), surface X-ray diffraction (SXR), low-energy electron diffraction (LEED).

**External routines/libraries:** Numpy, Scipy, Tomli, mpy4py

**Nature of problem:** Analysis of experimental measurement data

**Solution method:** Optimization, grid-based global search, Monte Carlo method

*Code Ocean capsule:* (to be added by Technical Editor)

## 1. Introduction

One major issue in computational physics is to construct a fast and reliable data-analysis method for experimental measurements. The data-analysis procedure is to obtain the target physical quantity  $X \equiv (X_1, X_2, \dots, X_n)$  from the experimentally observed data  $D \equiv (D_1, D_2, \dots, D_m)$ . A typical case is the inverse problem, in which  $D$  is caused by  $X$  and is written as a function of  $X$  ( $D = D_{\text{cal}}(X)$ ), which is referred to as a forward problem solver. The inverse problem is solved, in principle, by searching for the minimum of the objective function

$$F = F(X) \equiv d(D_{\text{cal}}(X), D), \quad (1)$$

where  $d(u, v)$  denotes a distance function between the two vectors  $u = (u_1, \dots, u_m)$  and  $v = (v_1, \dots, v_m)$ . Hereinafter the 2-norm form

$$d(u, v) \equiv \left( \sum_{i=1}^m (u_i - v_i)^2 \right)^{1/2}, \quad (2)$$

is used, except where indicated. The objective function  $F(X)$  may have local minima and may be affected by uncertainties due to the measurement conditions and the apparatus.

*Email addresses:* y-motoyama@issp.u-tokyo.ac.jp (Yuichi Motoyama), k-yoshimi@issp.u-tokyo.ac.jp (Kazuyoshi Yoshimi), hoshi@tottori-u.ac.jp (Takeo Hoshi)

Here, we focus on quantum-beam diffraction experiments for the structure determination of two-dimensional (2D) materials, since 2D materials hold great promise for industrial applications, such as next-generation electronic devices, and catalysts. Nowadays, the structure of 2D materials are measured by total-reflection high-energy positron diffraction (TRHEPD) [1–3], surface X-ray diffraction (SXRD) [4, 5] and low-energy electron diffraction (LEED) [6]. In these experiments,  $D$  is the diffraction intensity and  $X$  is the atom position in two-dimensional materials. However, 2D materials are generally more difficult to measure the structure (atom position) than three-dimensional materials, since the diffraction beam intensity of 2D materials is weak, and the types of structures are diverse.

The present paper reports that we have recently developed 2DMAT, an open-source data-analysis framework for two-dimensional material structures. The data-analysis methods are based on the above inverse-problem approach for TRHEPD, SXRD, and LEED experiments. In addition, 2DMAT is applicable to other problems if the user prepares an objective function  $F = F(X)$ . The software framework features parallel algorithms using the Message Passing Interface (MPI) for efficient data analysis not only by workstations with many-core CPU’s but also by supercomputers. An early-stage package was developed as a private program [7–9]. We then added several new features to the code and released the present package as an open-source software framework.

The remainder of the present paper is organized as follows. Section 2 gives an overview of the algorithms for the inverse problem. Section 3 explains the supported experiments and problems: TRHEPD, SXRD, LEED, and others. Section 4 explains the present software framework. Section 5 is devoted to examples. Finally, we summarize the present paper and comment on future utilities in Section 6.

## 2. Analysis algorithms for the inverse problem

This section is devoted to an overview of the following five analysis algorithms implemented in 2DMAT: (i) Nelder-Mead method [10, 11], (ii) grid search, (iii) Bayesian optimization (BO) method [12], (iv) replica exchange MC (REMC) method [13], and (v) population-annealing MC (PAMC) method [14]. These algorithms commonly use computation of the objective function  $F = F(X)$  in  $n$ -dimensional parameter space ( $X \equiv (X_1, \dots, X_n)$ ). For the latter four methods, MPI (MPI for Python [15–18]) can be used for parallel computation.

### 2.1. Nelder-Mead method

The Nelder-Mead optimization method, also known as the downhill simplex method [10, 11], is a gradient-free optimization method in which the gradient,  $\nabla_X F = (\partial F/\partial X_1, \partial F/\partial X_2, \dots, \partial F/\partial X_n)$ , is not required. The optimal solution is searched for by systematically moving pairs of  $n + 1$  coordinate points  $\{X^{(l)}\}_{l=1, \dots, n+1}$ , according to the value of the objective function  $F(X^{(l)})$  at each point  $X^{(l)}$ . In 2DMAT, the function `scipy.optimize.minimize` in `scipy` [19] is used, and the method is not parallelized.

### 2.2. Grid-search method

The grid-search method is an algorithm for searching for the minimum value of  $F(X)$  by computing  $F(X)$  for all of the candidate points in the parameter space prepared in advance. In 2DMAT, the set of candidate points is equally divided and automatically assigned to each process for trivial parallel computation.

### 2.3. Bayesian optimization method

The BO method is a black-box optimization method [12]. In BO, a surrogate model with a parameter set  $\theta$ ,  $G(X; \theta)$ , is trained by an observed dataset for representing  $F(X)$ . Then, by using the trained model  $G(X; \theta)$ , the next candidate  $X^*$  to be observed is obtained by optimizing an acquisition function calculated from the expectation value and the variance of  $G(X; \theta)$ . For example, the probability of improvement  $\text{PI}(X)$ , which is the probability that  $X$  becomes the new optimal solution when  $X$  is observed, is one of the widely-used acquisition functions. 2DMAT uses a BO library, `PHYSBO` [20, 21]. As for the grid-search method, `PHYSBO` requires the set of candidate points in advance but enables speed-up for yielding the next candidate by trivial parallelization.

### 2.4. Replica-exchange Monte Carlo method

Thus far, we have considered the optimization problem, i.e., the minimization of  $F(X; D)$  for determining the optimal value of  $X$  from the experimentally observed data  $D$ . Hereinafter, we will determine the conditional distribution of  $X$  under  $D$  (also known as the posterior probability distribution),  $\pi(X|D)$ . Then,  $\pi(X|D)$  is given by

$$\pi(X|D) = \frac{\pi(D|X)\pi(X)}{Z}, \quad (3)$$

where  $\pi(D|X)$  is the likelihood function,  $\pi(X)$  is the prior probability distribution of  $X$ , and  $Z = \int dX \pi(D|X)\pi(X)$  is the normalization factor. The likelihood  $\pi(D|X)$  is defined as  $\pi(D|X) = \exp(-F/\tau)$ . The given parameter  $\tau (> 0)$  is a measure of the tolerable uncertainty, which is called the ‘temperature’ based on the analogy of statistical physics. A constraint such as  $X_i^{(\text{lower})} \leq X_i \leq X_i^{(\text{upper})}$  is reduced to the uniform prior distribution in the region  $\pi(X)$ . The normalization factor  $Z$ , also called the partition function, is useful for choosing the proper model,  $D_{\text{cal}}(X)$ . By using these terms, the posterior probability distribution  $\pi(X|D; \tau)$  can be rewritten as

$$\pi(X|D; \tau) = \frac{\exp(-F(X; D)/\tau)}{Z\Omega}, \quad (4)$$

where  $\Omega$  is the volume of the region. Although it looks simple, it is generally difficult to evaluate  $\pi(X|D; \tau)$  for all of the parameter space when the number of parameters is large (curse of dimensionality).

Instead of a direct calculation of  $\pi(X|D; \tau)$  for entire region, the Markov chain MC (MCMC) method can be used to generate samples  $X^{(l)}$  with a probability proportional to  $\pi(X|D; \tau)$ . The MCMC method creates the next configuration  $X^{(t+1)}$  by a

small modification of the current configuration  $X^{(t)}$ . The temperature  $\tau$  is one of the most important hyper-parameters in MCMC sampling for the following reason. MCMC sampling can climb over a hill with a height of  $\tau$  but cannot easily escape from a valley deeper than  $\tau$ . Thus, we should increase the temperature in order to avoid becoming stuck in local minima. On the other hand, since walkers cannot see valleys smaller than  $\tau$ , the precision of the obtained result,  $F_{\min}$ , becomes approximately  $\tau$ , and decreasing the temperature is necessary in order to achieve more precise results. This dilemma indicates that we should tune the temperature carefully.

The replica-exchange MC (REMC) method [13] is an extended ensemble Monte Carlo method for overcoming this problem. In the REMC method,  $K$  independent systems (replicas) with different temperatures  $\tau_0, \tau_1, \dots, \tau_{K-1}$  are prepared, and the MCMC method is performed in parallel for each replica. After some updates,  $K/2$  pairs of all the replicas are created, and exchanging temperatures between replicas in each pair is attempted. This trial succeeds with some probability according to the detailed balance condition. After the efficiently long simulation, samples with the given temperature  $\tau_i$  gathered from all of the replicas follow a temperature-dependent distribution, i.e.,  $\pi(X|D; \tau_i)$ . In the REMC method, the temperature of each replica can change, and hence each replica can escape from local minima.

### 2.5. Population-annealing Monte Carlo method

The population-annealing MC (PAMC) method [14] is an extension of the simulated annealing (SA) method. The SA method starts performing the MCMC method at sufficiently high temperature and decreases the temperature gradually in order to search for the minimum of  $F(X)$ . However, the temperature-decreasing process, which suddenly changes the temperature, distorts the distribution of random walkers from equilibrium. This is because a burn-in process is needed for each temperature if the expectation values are wanted. The annealed importance sampling (AIS) method [22] compensates for this distortion by introducing an extra weight, i.e., the Neal-Jarzynskii (NJ) weight. The AIS method prepares  $N$  independent replicas and performs the SA method for these replicas in parallel. After  $N$  series of configurations are generated, the NJ weighted average of observables (e.g.,  $F(X)$  itself) is taken over all of the samples for each temperature. In the AIS method, the variance of the NJ weights increases as the simulation proceeds. This means that the effective number of samples becomes small, and, as a result, the calculation precision becomes worse. The PAMC method introduces resampling of replicas according to their NJ weights in order to reduce the variance of weights. After each resampling step, all of the NJ weights are reset to unity.

### 2.6. Comparison among the analysis methods

Finally, the five analysis methods are compared from the viewpoint of the application. The Nelder-Mead method consists of iterative local updates from an initial guess and tends to converge to a (local) minimum near the initial guess. The Nelder-Mead method is typically useful when an initial guess

is obtained by another analysis method. The grid search is reduced to trivial parallel computations and is useful if the total computational cost is bearable based on the computational resources of the user. The grid search, however, tends to be impractical with a large data dimension  $n = \dim(X)$ , since the number of grid points ( $N_{\text{grid}} \propto (N_{\text{grid}}^{\text{1D}})^n$ ) will be huge, as discussed, for example, in Section 4.4 of Reference [9]. The BO method can realize an efficient iterative search to obtain the optimal point  $X^{(\text{opt})}$  by setting a surrogate model and an initial dataset generated by a random search. The two MC methods generally require a large number of sampling points but give a histogram of the posterior probability density as a unique stationary state. The posterior probability density is crucial when the uncertainty is estimated based on the experimental conditions and apparatus, as in Reference [23, 24] for the SXR experiment.

The difference between the REMC and PAMC methods appears in the typical number of parallel (MPI) processes  $N_p$ . The REMC method is a parallel computation among various tolerable uncertainty parameters  $\{\tau_i\}_i$  and the typical number of possible parallel processes  $N_p$  is  $N_p = 10 - 10^2$ . The PAMC method is a parallel computation among different replicas at a given value of the tolerable uncertainty parameter  $\tau = \tau_i$  and the typical number of possible parallel processes  $N_p$  is  $N_p = 10^3 - 10^5$  or more. A practical comparison between the REMC and PAMC methods is ongoing on supercomputers.

## 3. Supported experiments and objective functions

This section is devoted to an overview of the supported experiments and problems. 2DMAT is applicable to various experiments and problems by preparing a proper forward problem solver  $D_{\text{cal}}(X)$ . The present package supports TRHEPD, SXR, and LEED experiments, as explained in Sections 3.1, 3.2, and 3.3, respectively. The present package also supports several analytic test functions for  $F(X)$ , and users can define a user-defined function  $F(X)$ , which will be explained in Sections 3.4 and 3.5.

### 3.1. Total-reflection high-energy positron diffraction (TRHEPD)

The analysis of TRHEPD data is realized, when `sim-threpd-rheed` [25–27], an open-source simulator written in Fortran, is installed. Total-reflection high-energy positron diffraction is a novel experimental probe for two-dimensional materials and has been actively developed in the last decade at large-scale experimental facilities at the Slow Positron Facility (SPF), Institute of Materials Structure Science (IMSS), High-Energy Accelerator Research Organization (KEK) [1–3, 28, 29]. Details are provided in review studies [1–3].

### 3.2. Surface X-ray diffraction

The analysis of SXR data is realized when `sxrddcalc` [30, 31], an open-source simulator written in the C language, is installed. Surface X-ray diffraction has been used for decades

for structure analysis experiments involving two-dimensional materials. Details are provided in review studies [4, 5]. It is noted that several other SXR D simulators, like ANA-ROD [32, 33] and CTR-structure [23, 24, 34], are available online.

### 3.3. Low-energy electron diffraction

The analysis of LEED data is realized by installing SATLEED [6], a well-known simulator written in Fortran, as the forward problem solver  $D_{\text{cal}}(X)$ . Low-energy electron diffraction has been used for decades for structure analysis experiments involving two-dimensional materials. Details are provided in review studies [6]. Low-energy electron diffraction data was analyzed by SATLEED in numerous studies such as Ref. [35]. Note that the LEED simulator is also applicable to low-energy positron diffraction (LEPD) [36, 37], recently developed for structure determination of two-dimensional materials.

### 3.4. Analytic test functions

Several well-known analytic test functions, such as the Rosenbrock function [38], the Ackley function [39], and the Himmelblau function [40] are also implemented as the objective function  $F(X)$  in order to demonstrate the algorithms in Section 2. For example, the Himmelblau function is given as

$$F(x, y) = (x^2 + y - 11)^2 + (x + y^2 - 7)^2, \quad (5)$$

and the minimum value of  $F = 0$  appears at  $(x, y) \approx (3.00, 2.00), (-2.81, 3.13), (-3.78, -3.28),$  and  $(3.58, -1.85)$ .

### 3.5. User-defined objective functions

Users can implement and analyze any objective function  $F(X)$ . For example, in a previous study [41], the REMC algorithm in 2DMAT was used as the performance prediction method for a massively parallel numerical library for a generalized eigenvalue problem. This paper shows a method by which to predict the elapsed time  $T$  for the numerical library as a function of the number of nodes used  $P$  ( $T = T(P)$ ) and focuses on extrapolation to larger values of  $P$ . The teacher dataset is the set of measured elapsed times for various numbers of nodes  $\{T_{\text{exp}}(P_i)\}_{i=1, \dots, \nu}$ . The present paper proposed a model of the elapsed time  $T_{\text{cal}}(P, X)$  with a parameter set  $X = (C_1, C_2, \dots, C_n)$ . The objective function to be minimized is the relative error

$$F(X) = \sum_i^{\nu} \frac{|T_{\text{cal}}(P_i, X) - T_{\text{exp}}(P_i)|^2}{|T_{\text{exp}}(P_i)|^2}. \quad (6)$$

## 4. Software

2DMAT is a framework for applying a search algorithm to a forward problem solver  $D_{\text{cal}}(X)$  in order to find the optimal solution of  $F(X)$ , such as determining the optimized atomic positions. A prototype package of 2DMAT was developed as a private program [7–9]. We then added several new features to the code and released 2DMAT as an open-source software framework. The structure of 2DMAT is shown in Fig. 1.

2DMAT requires one input file with the TOML format [42] and reference files for the forward problem solver, for example, the experimental data to be fitted. The input file has the following six sections<sup>1</sup>:

1. The [base] section specifies the basic parameters.
2. The [solver] section specifies the parameters related to the forward problem solver.
3. The [algorithm] section specifies the parameters related to the algorithm.
4. The [runner] section specifies the parameters of Runner, which bridges the Algorithm and the Solver.
5. The [mapping] section defines the mapping from a parameter searched by the Algorithm to a parameter used in the forward problem solver.
6. The [log] section specifies parameters related to logging of solver calls.

In addition, reference files such as the target data  $D$  to be fitted and basic input files for forward problem solver are needed. After preparing these files, the optimized parameters  $X_{\text{opt}}$  can be searched for by running 2DMAT.

After finishing the calculation, 2DMAT outputs the `time.log`, which describes the total calculate time, and `runner.log`, which contains log information about solver calls. In addition, output files for each forward solver and the algorithm are saved. For details, see the manual for 2DMAT. Below, the installation and usage of 2DMAT are introduced through a demonstration.

### 4.1. Install

2DMAT is written in Python and requires Python 3.6.8 or higher. Installing 2DMAT requires the python packages `tomli` [43] and `numpy` [44]. In addition, as optional packages, `scipy` [19], and `physbo` [21] are required the Nelder-Mead method, and Bayesian optimization, respectively. If users want to perform a parallel calculation, `mpi4py` [18] is also required. These packages are registered in PyPI, which is a public repository of Python software. Since 2DMAT is also registered in PyPI, users can install 2DMAT simply by typing the following command:

```
$ python3 -m pip install py2dmat
```

The sample files can be downloaded from the official site for 2DMAT. Using git, all files will be downloaded by typing the following command:

```
$ git clone https://github.com/issp-center-dev/2DMAT
```

Recently, some of authors have developed the MateriApps Installer[45], a scripting tool that provides a computing environment for using various software packages. Users can also be used to install 2DMAT with setting the necessary libraries.

Note that forward problem solvers used in `py2dmat`, such as `sim-trhepd-rheed` and `sxrd`, must be installed separately when users want to use these solvers. Information on each solver, available from official websites, is in the 2DMAT manual.

<sup>1</sup>A section, called a 'table' in TOML, is a set of parameters specified in the name = value format.

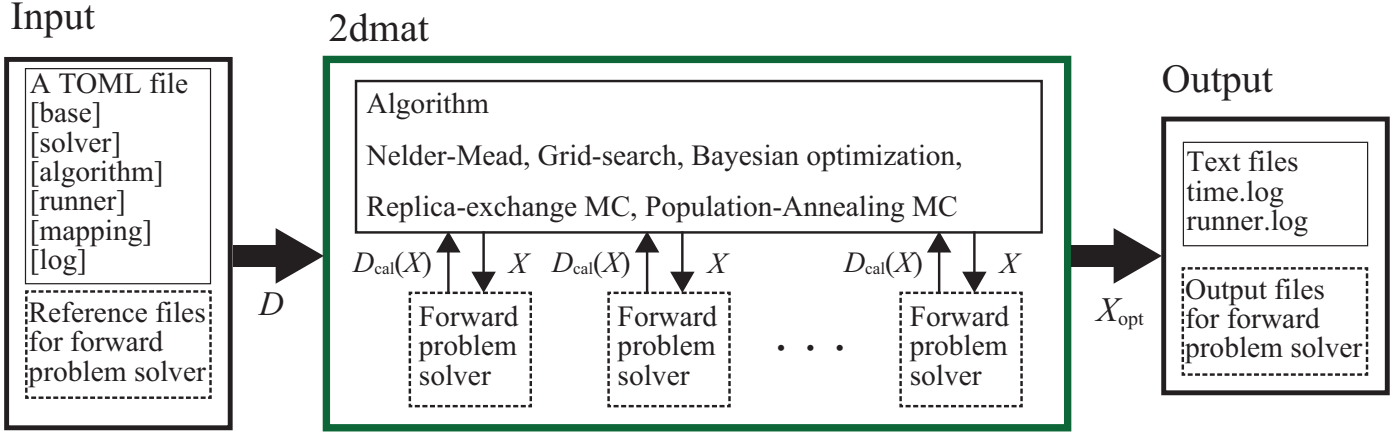


Figure 1: Schematic calculation flow for 2DMAT. The data to be fitted,  $D$ , are given by the input file. When the target quantity  $X$  is given, the forward problem solver calculates the numerical data  $D_{\text{cal}}(X)$ . Through an analysis algorithm, a candidate solution  $X$  is proposed to minimize  $|D - D_{\text{cal}}(X)|$ . When the analysis process is finished, the optimal point  $X_{\text{opt}}$  is output. In the MC method, the posterior probability density can be output as a histogram.

#### 4.2. Usage

Let us introduce the use of 2DMAT through a sample demonstration. The input file for this sample, `input.toml`, is located in the `sample/analytical/bayes` directory and shown as follows:

```
[base]
dimension = 2
output_dir = "output"

[algorithm]
name = "bayes"
seed = 12345

[algorithm.param]
max_list = [6.0, 6.0]
min_list = [-6.0, -6.0]
num_list = [61, 61]

[algorithm.bayes]
random_max_num_probes = 20
bayes_max_num_probes = 40

[solver]
name = "analytical"
function_name = "himmelblau"
```

In the `[base]` section, the dimension of parameters to be optimized and the output directory are specified by variables `dimension` and `output_dir`, which are set as 2 and `output`, respectively. In the `[algorithm]` section, the search algorithm and the seed of the random number generator are specified by parameters names and `seed`, which are set as

"bayes" and 12,345, respectively. There are subsections depending on the search algorithm. In the case of selecting the algorithm "bayes", there are `param` and `bayes` subsections. In the `param` subsection, the search region can be specified by setting the maximum and minimum values, `max_list` and `min_list`, and the specified space is equally divided by the parameter `num_list`. In this example, the two-dimensional space  $[-6, 6]$ ,  $[-6, 6]$  for the 61 divided parameters is searched. In the `bayes` subsection, the number of random samplings to be taken before Bayesian optimization `random_max_num_probes` and the number of steps to perform Bayesian optimization `bayes_max_num_probes` are specified. The default score function (acquisition function) is set as Thomson sampling. If the user wants to use expected improvement (EI) or probability of improvement (PI) as the score, then the parameter `score` is available (e.g., `score = "EI"`). In the `[solver]` section, the forward problem solver is specified as the `himmelblau` function, Eq. (5), as defined in the `analytical` solver using `name` and `function_name`.

After preparing the input file, the calculation will be performed in two ways. The first is the `py2dmat` command, which is installed via `pip install`. Here, `py2dmat` takes one argument, the name of the input file, as follows:

```
$ py2dmat input.toml
```

The second is to use the python script `py2dmat_main.py`, which is located in the `src` directory. The command for execution is given as follows (here, we assume that the current directory is `sample/analytical/bayes`):

```
$ python3 ../../../../src/py2dmat_main.py input.toml
```

The only difference between these methods is which python package will be used. The former uses the installed python

package, and the latter uses the source files located in `src/py2dmat`. After finishing the calculation, the following files are output to the output directory. In `BayesData.txt`, step  $i$ , the best parameter  $X_{\text{best}}$ , and  $F(X_{\text{best}})$ , as well as the action  $X_i$ , and  $F(X_i)$  at the  $i$ -th step are output as shown below.

```
#step x1 x2 fx x1_action x2_action fx_action
0 -2.4 -0.7999999999999998 ...
1 -2.4 -0.7999999999999998 ...
...
57 3.60000000000000014 -1.7999999999999998 ...
58 3.60000000000000014 -1.7999999999999998 ...
59 3.60000000000000014 -1.7999999999999998 ...
```

In this case, we can see that the optimal parameter at step 60 is  $(3.6, -1.8)$  around  $(3.58, -1.85)$ , one of the exact minimum points of  $F(X)$  defined in Eq. (5).

We can easily apply another algorithm to solving the same inverse problem by editing `[algorithm]` section in the input file. For example, PAMC method can be applied when we change the `[algorithm]` section in the input file as follows:

```
[algorithm]
name = "pamc"
seed = 12345

[algorithm.param]
max_list = [6.0, 6.0]
min_list = [-6.0, -6.0]
unit_list = [0.05, 0.05]

[algorithm.pamc]
bmin = 0.0
bmax = 10.0
Tnum = 20
Tlogspace = false
numsteps_annealing = 20
nreplica_per_proc = 130
resampling_interval = 4
```

In this case, the number of replicas was set to  $N_{\text{replica}} = 3, 120$ , and the number of annealing steps or the number of temperature values was set to  $K = 20$ . The initial and final temperatures were  $\tau_0^{-1} = 0$  and  $\tau_{K-1}^{-1} = 10$ , respectively. The intermediate temperatures  $\{\tau_j\}_{j=1, \dots, K-2}$  were prepared to discretize  $[\tau_0^{-1}, \tau_{K-1}^{-1}]$  uniformly, i.e.,

$$\tau_j^{-1} = \tau_0^{-1} + (\tau_{K-1}^{-1} - \tau_0^{-1}) \frac{j}{K-1}. \quad (7)$$

At each temperature ( $\tau = \tau_j$ ),  $N_{\text{MCMC}}^{(\text{tmp})} = 20$  MCMC steps were carried out. The total number of MCMC steps for each replica was  $K \times N_{\text{MCMC}}^{(\text{tmp})} = 20 \times 20 = 400$ . The resampling process occurred every four annealing steps. Figure 2 shows the resultant histogram of the probability density at (a)  $\tau^{-1} = \tau_1^{-1} \approx 0.53$  and (b)  $\tau^{-1} = \tau_{19}^{-1} = 10$ . The histograms in Figures 2(a) and 2(b) were drawn with a bin width of  $h_{\text{bin}} = 0.1$ . Figure 2(b) confirms that the PAMC analysis detects the four global minima correctly. For details of the algorithms and their parameter settings, please refer to the 2DMAT official manual.

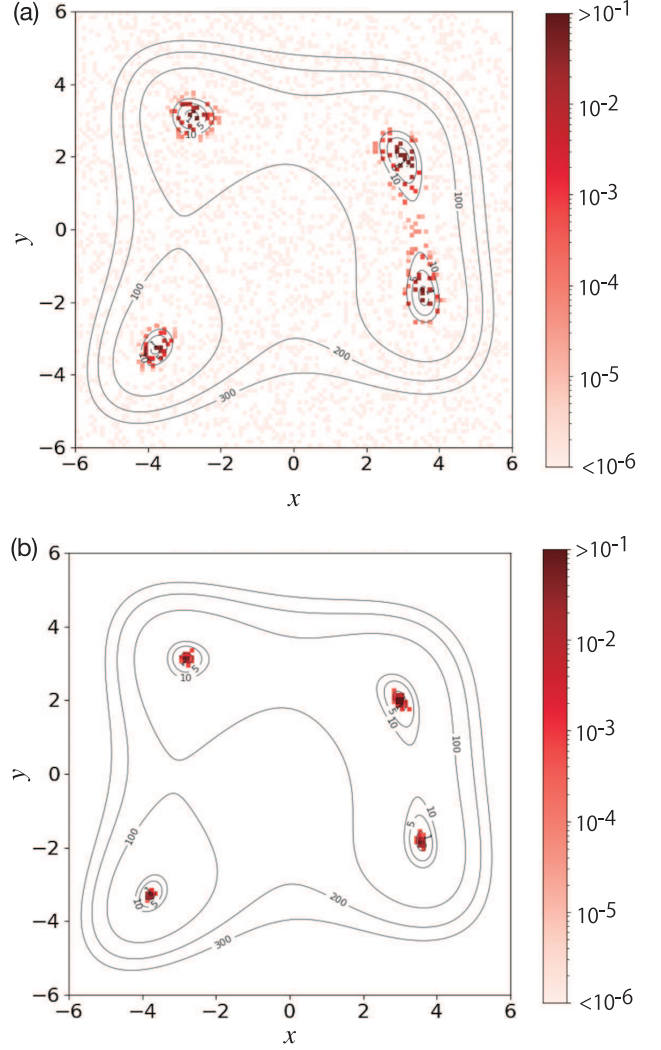


Figure 2: Population-annealing Monte Carlo (PAMC) analysis of Himmelblau function. Histograms of probability density  $\pi(x, y; \tau)$  are shown at (a)  $\tau^{-1} \approx 0.53$  and (b)  $\tau^{-1} \approx 10$ . The contour of  $F$  is also plotted as a guide for the eye.

#### 4.3. User-defined objective function

The simplest way to define a user-defined objective function  $F(X)$  is to add the function to the analytical solver, which is for the benchmark test. This solver is defined in the `src/py2dmat/solver/analytical.py` file, and hence a new problem can be added simply by editing this file. When adding the function, the function can be analyzed by invoking the `src/py2dmat.main.py` script.

Another way is to use the function solver, which can register a python function as  $F(X)$ . The following simple script (`sample/user_function/simple.py`) shows an example for a grid search of a user-defined objective function  $F(X) = \sum_i^N X_i^2/N$ :

```
1 import numpy as np
2 import py2dmat
3 import py2dmat.util.toml
4 import py2dmat.algorithm.mapper_mpi as pm_alg
5 import py2dmat.solver.function
6
```

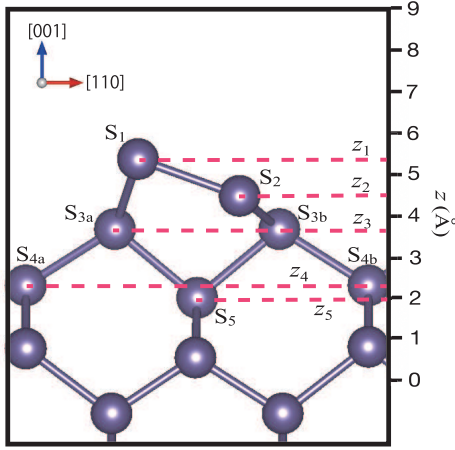


Figure 3: Side view of the Ge(001)-c(4×2) surface structure. The  $z$  coordinates of the first, second, third, fourth and fifth surface layers are denoted as  $z_1$ ,  $z_2$ ,  $z_3$ ,  $z_4$  and  $z_5$ , respectively.

```

7 def my_objective_fn(x: np.ndarray) -> float:
8     return np.mean(x * x)
9
10 file_name = "input.toml"
11 inp = py2dmat.util.toml.load(file_name)
12 info = py2dmat.Info(inp)
13 solver = py2dmat.solver.function.Solver(info)
14 solver.set_function(my_objective_fn)
15 runner = py2dmat.Runner(solver, info)
16 alg = pm_alg.Algorithm(info, runner)
17 alg.main()

```

At line 14, `solver.set_function` registers a function `my_objective_fn` as the objective function. In this way, the original source code of Py2dmat does not need to be edited.

## 5. Examples of TRHEPD data analysis

### 5.1. Analysis of artificial TRHEPD data

In this subsection, all of the analysis algorithms in Section 2, except for the PAMC algorithm, are demonstrated with an example of the artificial generated TRHEPD data. The application of the PAMC method is skipped in this section, because the PAMC and REMC methods calculate, commonly, the posterior probability density  $\pi(X|D; \tau_i)$ , and the resultant figures for the PAMC method are almost the same as for the REMC method.

The present example for the TRHEPD experiment is the Ge(001)-c(4 × 2) surface, a famous semiconductor surface. Hereinafter, the  $z$  axis is defined as being normal to the material surface. Figure 3 shows a side view of the surface structure. The horizontal view is found, for example, in Fig. 3(b) of Reference [8]. The first and second surface atoms are denoted by  $S_1$  and  $S_2$ , respectively, and form an asymmetric dimer. The third surface atoms are denoted by  $S_{3a}$  and  $S_{3b}$ . The fourth surface atoms are denoted by  $S_{4a}$  and  $S_{4b}$ . The fifth surface atom is denoted by  $S_5$ . The  $z$  coordinates of the first layer ( $S_1$ ), the second layer ( $S_2$ ), the third layer ( $S_{3a}$  and  $S_{3b}$ ), the fourth layer ( $S_{4a}$  and  $S_{4b}$ ) and the fifth layer ( $S_5$ ) are denoted as  $z_1$ ,  $z_2$ ,  $z_3$ ,  $z_4$  and  $z_5$ , respectively.

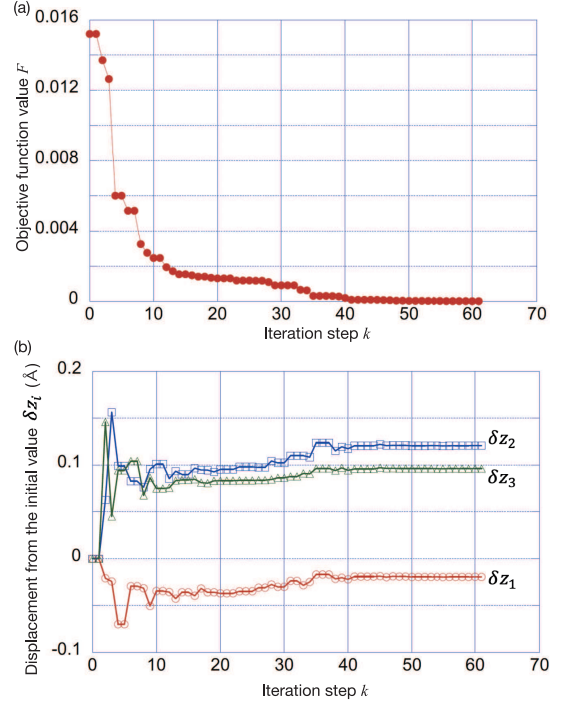


Figure 4: Nelder-Mead analysis of TRHEPD experiment for Ge(001)-c(4 × 2) surface. (a) The objective function  $F = F(z_1^{(k)}, z_2^{(k)}, z_3^{(k)})$  and (b) the deviations from the initial values  $\delta z_i^{(k)} = z_i^{(k)} - z_i^{(0)}$  ( $i = 1, 2, 3$ ) are plotted as functions of the iteration step  $k$  ( $= 0, 1, 2, \dots$ ).

The experimental data are set to be those for the one-beam condition [2, 46], the experimental condition for the determination of the  $z$  coordinates of the atom positions. The present analysis was carried out with artificial reference data, instead of real experimental data, as in the previous paper [8]. The reference data were generated by a simulation with reference positions of  $(z_1, z_2, z_3) = (z_1^{(\text{ref})}, z_2^{(\text{ref})}, z_3^{(\text{ref})}) \approx (5.231 \text{Å}, 4.371 \text{Å}, 3.596 \text{Å})$  [8, 47].

The objective function is expressed as  $F = F(z_1, z_2, z_3)$ . When the values of  $z_1$  and  $z_2$  are replaced with each other, the objective function  $F(z_1, z_2, z_3)$  is unchanged ( $F(z_2, z_1, z_3) = F(z_1, z_2, z_3)$ ), owing to the symmetry of the structure. Therefore, we do not lose generality by assuming the constraint  $z_1 \geq z_2$ .

#### 5.1.1. Nelder-Mead analysis

The Nelder-Mead method was applied to the analysis of the Ge(001)-c(4 × 2) surface in a previous study [8], in which the initial values were chosen to be  $(z_1, z_2, z_3) = (z_1^{(0)}, z_2^{(0)}, z_3^{(0)}) \equiv (5.25 \text{Å}, 4.25 \text{Å}, 3.50 \text{Å})$ . Figure 4(a) shows that the objective function  $F$  decreases monotonically through the iterative optimization steps  $k$  ( $= 0, 1, 2, \dots$ ) and reaches the convergence point  $(z_1, z_2, z_3) = (z_1^{(\text{ref})}, z_2^{(\text{ref})}, z_3^{(\text{ref})})$  after  $k = 61$  iterative steps. Figure 4(b) shows the deviations from the initial values  $\delta z_i^{(k)} = z_i^{(k)} - z_i^{(0)}$  ( $i = 1, 2, 3$ ) as functions of the iteration step  $k$ . It can be seen that  $\delta z_i^{(k)}$  is small ( $|\delta z_i^{(k)}| \leq 0.15 \text{Å}$ ) for the converged structure. The files for the calculation are stored in the `sample/py2dmat/minsearch/` directory.

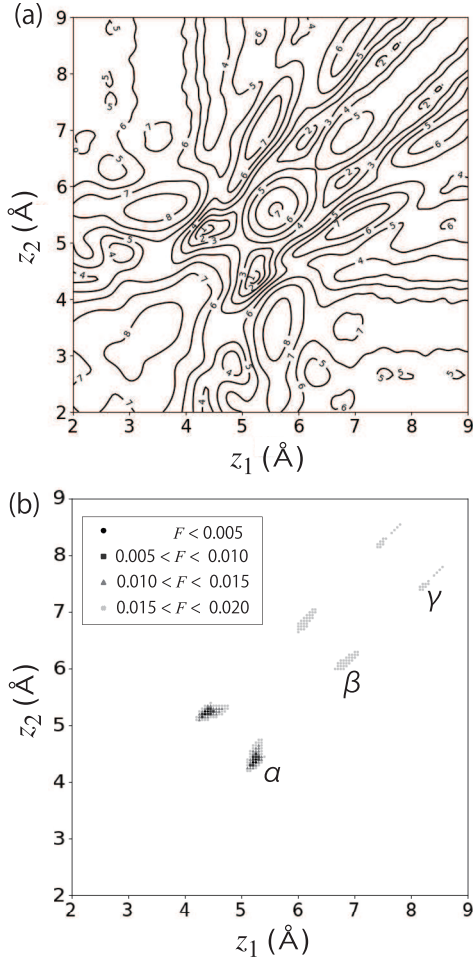


Figure 5: Grid-search analysis of TRHEPD experiment for Ge(001)-c( $4 \times 2$ ) surface. (a) Contour plot of the objective function  $F(z_1, z_2)$  using the grid-search data. The isovalues are shown as  $100 \times F$ . (b) Objective function  $F(z_1, z_2)$  on the selected grid data that satisfy  $F < 0.005$  (circles),  $0.005 < F < 0.010$  (squares),  $0.010 < F < 0.015$  (triangles), and  $0.015 < F < 0.020$  (crosses).

### 5.1.2. Grid-search analysis

A grid search was applied to the analysis of the Ge(001)-c( $4 \times 2$ ) surface in a previous study [8], in which the grid points were on a  $(z_1, z_2, z_3)$  space with a grid interval of  $h = 0.25 \text{ \AA}$ .

Figure 5 shows the results of the grid search on a  $(z_1, z_2)$  space with a grid interval of  $h = 0.05 \text{ \AA}$ , where  $z_3$  is fixed at  $z_3 = z_3^{(\text{ref})}$ . The grid range is  $L_{\text{min}} \equiv 2 \text{ \AA} \leq z_1, z_2 \leq L_{\text{max}} \equiv 9 \text{ \AA}$ , and the number of the grid points on the  $z_1$  or  $z_2$  axis is  $N_{\text{grid}}^{(1D)} = (L_{\text{max}} - L_{\text{min}})/h + 1 = 141$ . The total number of grid points is  $N_{\text{grid}} = (N_{\text{grid}}^{(1D)})^2 = 141^2 = 19,881$ . As a result, the grid minimum points are obtained  $(z_1, z_2) = (5.25 \text{ \AA}, 4.4 \text{ \AA}), (4.4 \text{ \AA}, 5.25 \text{ \AA})$  that give the minimum value of  $F = 0.003$ . The grid minimum point  $(z_1, z_2) = (5.25 \text{ \AA}, 4.4 \text{ \AA})$  is close to the true minimum point  $(z_1^{(\text{ref})}, z_2^{(\text{ref})}) \approx (5.231 \text{ \AA}, 4.371 \text{ \AA})$ . To obtain a finer solution than the grid minimum point, the Nelder-Mead method, in which the initial point is chosen to be the grid minimum point, can be used.

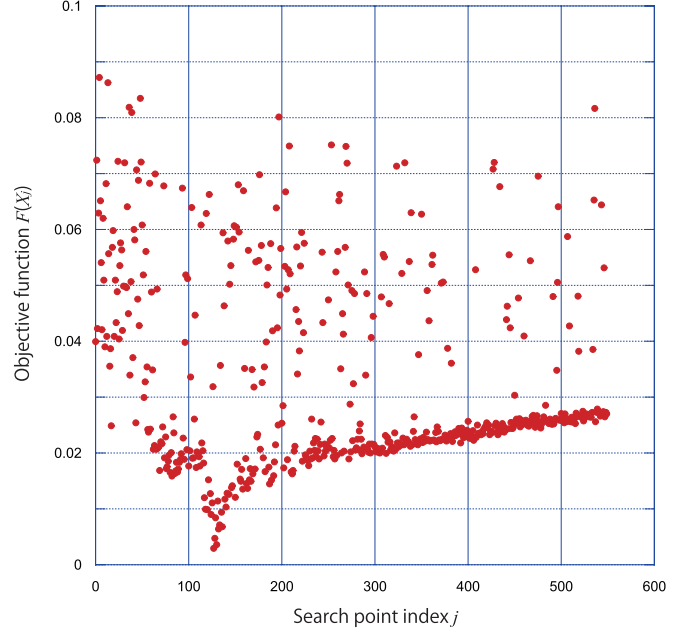


Figure 6: Objective function at search points  $F(z_1^{(j)}, z_2^{(j)})$  with  $j = 0, 1, 2, \dots, 549$  in Bayesian optimization (BO) analysis of TRHEPD data for Ge(001)-c( $4 \times 2$ ) surface.

Figure 5(a) plots the contour of  $F$  using the grid search data and indicates that the objective function  $F(z_1, z_2)$  has many local minima. Figure 5(b) picks out the grid points that satisfy the condition  $F < 0.02$ , because these points are candidate solutions in practical data analysis [2, 9]. Three local regions that contain (local) minima are found within the condition  $z_1 \geq z_2$  and are denoted as  $\alpha$ ,  $\beta$ , and  $\gamma$ . The region  $\alpha$  contains the grid minimum point  $(z_1, z_2) = (5.25 \text{ \AA}, 4.4 \text{ \AA})$  with  $F \approx 0.003$ , while the regions  $\beta$  and  $\gamma$  contain local minima with  $0.01 < F < 0.02$ .

Note that the three regions,  $\alpha$ ,  $\beta$ , and  $\gamma$ , are almost linearly distributed and satisfy the relation  $(z_1 - z_2) \approx (\text{constant})$ , which is a common property of TRHEPD. Similar results have also been obtained for the  $\text{Si}_4\text{O}_5\text{N}_3 / 6\text{H-SiC}(0001)$ -( $\sqrt{3} \times \sqrt{3}$ )  $\text{R}30^\circ$  surface, as shown in Fig. 3(a) of Reference [9]. This stems from the fact that the interaction of positron waves scattered from the first and second atomic layers contributes significantly to the diffraction signal, and the objective function  $F(z_1, z_2)$  is quite sensitive to the distance between the first and second atomic layers  $(z_1 - z_2)$  [9].

### 5.1.3. Bayesian optimization analysis

The BO analysis was carried out using a similar grid to that in Section 5.1.2, but the grid points were prepared only under the constraint  $z_1 \geq z_2$ . Thus, the total number of grid points is  $N_{\text{grid,BO}} = (N_{\text{grid}}^{(1D)})(N_{\text{grid}}^{(1D)} + 1)/2 = 141 \times 142/2 = 10,011$ .

Figure 6 plots the objective function  $F(z_1^{(j)}, z_2^{(j)})$  as a function of the search point index  $j = 0, 1, 2, \dots, 549$ . The initial  $n_{\text{rand}} = 50$  search points ( $j = 0, \dots, 49$ ) were generated using a random search. Then, the search points with  $j = 50, 51, \dots$  were generated iteratively using the BO algorithm. Figure 6 indicates that the grid minimum point  $F(z_1=5.25 \text{ \AA}, z_2=4.4$



$\text{\AA}$ )=0.003 appears at  $j=127$ . The number of search points  $n_{\text{opt}} = 127$  is much smaller than the total number of grid points  $N_{\text{grid,BO}} = 10,011$  ( $n_{\text{opt}} \ll N_{\text{grid,BO}}$ ), which shows the efficiency of the BO method.

Figure 7 shows the search points  $(z_1^{(j)}, z_2^{(j)})$  that appear in the BO analysis with (a)  $j \leq 49$ , (b)  $j \leq 127$ , and (c)  $j \leq 549$ . Figure 7 indicates that the search points cover the region  $\beta$  at first, as seen in Figure 7(b), and then cover the regions  $\alpha$  and  $\gamma$  later, as shown in Fig. 7(c).

#### 5.1.4. Replica-exchange Monte Carlo analysis

Figure 8 shows the results of the REMC method. In this example, we used  $K = 36$  replicas and prepared datasets for temperature  $\{\tau_j\}_{j=0,\dots,K-1}$  as follows. The maximum and minimum temperatures were  $\tau_0 = 0.1$  and  $\tau_{K-1} = 0.001$ , respectively, and the other values  $\{\tau_j\}_{j=1,\dots,K-2}$  were prepared to discretize  $[\tau_0, \tau_{K-1}]$  uniformly on a log scale, i.e.,

$$\tau_j = \tau_0 \times \left( \frac{\tau_{K-1}}{\tau_0} \right)^{\frac{j}{K-1}}. \quad (8)$$

The total number of MCMC steps was  $N_{\text{MCMC}} = 50,000$  for each replica. The temperature-exchange process occurred every 50 MCMC steps. Figure 8 shows the posterior distributions  $\pi(z_1, z_2 | D; \tau)$ , as histograms, at (a)  $\tau = \tau_0 = 0.1$ , (b)  $\tau = \tau_{27} \approx 0.0029$  and (c)  $\tau = \tau_{35} = 0.001$ . The histograms were constructed without the ‘burn-in’ data at the early  $N_{\text{MCMC}}/2$  MCMC steps and were drawn with a bin size of  $h_{\text{bin}} = 0.05 \text{ \AA}$ . The histogram in Fig. 8(b) indicates that the objective function has two minima. In Figs. 8(b) and 8(c), the histogram can be confirmed to be symmetric  $\pi(z_1, z_2 | D; \tau) \approx \pi(z_2, z_1 | D; \tau)$  owing to the symmetry of the objective function ( $F(z_1, z_2) = F(z_2, z_1)$ ).

## 5.2. Analysis of experimental TRHEPD data

The present subsection is devoted to the analysis of the experimental TRHEPD data. Several studies for other materials are ongoing.

### 5.2.1. Ge(001)-c( $4 \times 2$ ) surface

Very recently, one of the authors (I. M.) carried out the TRHEPD experiment for Ge(001)-c( $4 \times 2$ ) surface. The sample preparation and the measurement condition are explained as follows. The sample substrate ( $5 \times 10 \times 0.5 \text{ mm}^3$ ) was cut from a mirror-polished Ge(001) wafer. The surface was cleaned by a few cycles of  $0.5 \text{ keV Ar}^+$  sputtering ( $\sim 5 \times 10^{-4} \text{ Pa}$ ,  $673 \text{ K}$ ,  $15 \text{ min}$ ) followed by annealing ( $853 \text{ K}$ ,  $10 \text{ min}$ ) in a TRHEPD measurement chamber [9, 28, 29], after which cleanliness and well-ordered periodicity of the surface were confirmed by reflection high-energy electron diffraction patterns. The TRHEPD experiment was performed using a positron beam of  $10 \text{ keV}$ . The incident azimuth was set at  $22.5^\circ$  off the  $[1\bar{1}0]$  direction (i.e., the one-beam condition [2, 46]). The glancing angle was varied from  $0.5^\circ$  to  $6.5^\circ$ .

The experimental data was analyzed by the Nelder-Mead method using 2DMAT. The iterative procedure was performed for the five variables  $\{z_i\}_{i=1,5}$  in Fig. 3, until the objective function  $F = F(z_1, z_2, z_3, z_4, z_5)$  converges within the criteria

$\Delta F = 5 \times 10^{-4}$ . The initial structure was set to be the one determined by LEED experiment [47]. Figure 9(a) shows the objective function  $F^{(k)} = F(z_1^{(k)}, z_2^{(k)}, z_3^{(k)}, z_4^{(k)}, z_5^{(k)})$  as the function of the iterative step  $k (= 0, 1, \dots, 24)$ . As a result, the objective function  $F^{(k)}$  decreases from  $F^{(0)} = 1.96 \times 10^{-2}$  at the initial structure into  $F^{(24)} = 1.40 \times 10^{-2}$  at the converged structure. Figure 9(b) shows the deviation of the variables  $\{z_i\}_{i=1,5}$  from the initial values  $\delta z_i^{(k)} = z_i^{(k)} - z_i^{(0)}$  as the function of the iteration step  $k$ . Here one finds that the difference between the initial and final structures was approximately  $0.15 \text{ \AA}$  or less. In other words, the structures determined by the TRHEPD and LEED experiments agree with a small ( $0.1 \text{ \AA}$ -scale) difference. Figure 10 shows the calculated rocking curves in the initial and converged structures, together with the experimental data. The calculated rocking curves in the converged structure agrees with the experimental data better than that of the initial structure.

It is noted that, among existing TRHEPD researches (Refs. [2, 9] and references therein), a structure is accepted as a final solution, when the objective function value is less than  $0.02$  ( $F \leq 0.02$ ). The present result demonstrates that the TRHEPD diffraction data is sensitive to a small ( $0.1 \text{ \AA}$ -scale) difference in the coordinates.

### 5.2.2. Si<sub>4</sub>O<sub>5</sub>N<sub>3</sub> / 6H-SiC(0001)-( $\sqrt{3} \times \sqrt{3}$ ) R30° surface

A previous paper [9] reports that 2DMAT was used in the data analysis of TRHEPD experiment for Si<sub>4</sub>O<sub>5</sub>N<sub>3</sub> / 6H-SiC(0001)-(  $\sqrt{3} \times \sqrt{3}$ ) R30° surface, a novel two-dimensional semiconductor. The trial atomic positions were optimized by the Nelder-Mead method, in which the value of the objective function decreases from  $F = 2.28 \times 10^{-2}$  into  $F = 0.91 \times 10^{-2}$ . In addition, a grid search was carried out for a local region near the optimized position, so as to investigate the properties of the objective function in the local region.

## 6. Summary and future utilities

A general-purpose open-source software framework 2DMAT has been developed for analysis of experimental data using an inverse problem approach. The framework provides five analysis algorithms: the Nelder-Mead optimization, the grid search, the Bayesian optimization, the replica-exchange Monte Carlo, and the population-annealing Monte Carlo methods. Thus, users can choose an appropriate analysis method according to the purpose and can construct a multi-stage scheme, in which a single method is carried out first, and then other methods are performed. The current version of 2DMAT supports analysis of several experiments; TRHEPD, SXRD, and LEED data by offering adapters for the external software packages for simulating these experiments. 2DMAT is designed to define the objective function by users. Thus, by adding the appropriate objective function, many experimental measurements can be analyzed using 2DMAT.

Finally, we comment on the future utilities of 2DMAT. Several application studies beyond those in this paper are ongoing and several types of the studies are picked out below: The first type of the ongoing studies is the the analysis of the experimental data of SXRD and LEED. In particular, 2DMAT will

enable us a fruitful analysis, when we perform multiple types of the diffraction experiments on a specimen and analyze the results seamlessly. The second type of the ongoing studies is the prediction of material properties, which is realized by *ab initio* calculations with the determined atomic positions. For this purpose, some of the present authors developed a tool that converts the atomic position data file used in TRHEPD analysis into the file of Quantum Espresso, a famous *ab initio* software package [25, 27, 48]. The third type of the ongoing studies is application to other problems beyond 2D materials, where we construct a user-defined problem, as explained in Sec. 3.5. With these features and possible future utilities, we expect that 2DMAT becomes a useful data-analysis framework in material science and other scientific fields.

## Acknowledgement

We would like to acknowledge support for code development from the “Project for advancement of software usability in materials science (PASUMS)” by the Institute for Solid State Physics, University of Tokyo. The present research was supported in part by a Grant-in-Aid for Scientific Research (KAKENHI) from the Japan Society for the Promotion of Science (19H04125, 20H00581). 2DMAT was developed using the following supercomputers: the Ohtaka supercomputer at the Supercomputer Center, Institute for Solid State Physics, University of Tokyo; the Fugaku supercomputer through the HPCI projects (hp210083, hp210267); the Oakforest-PACS supercomputer as part of the Interdisciplinary Computational Science Program in the Center for Computational Sciences, University of Tsukuba; the Wisteria-Odyssey supercomputer at the Information Technology Center, University of Tokyo; and the Laurel2 supercomputer at the Academic Center for Computing and Media Studies, Kyoto University. The present research was also supported in part by JHPCN project (jh210044-NAH). We would like to acknowledge Takashi Hanada, Wolfgang Voegeli, Tetsuroh Shirasawa, Rezwan Ahmed, and Ken Wada for fruitful discussions on the diffraction experiments, and Daishiro Sakata, Koji Hukushima, Taisuke Ozaki, and Osamu Sugino for fruitful discussions on the code.

## References

- [1] C. Hugenschmidt, Surf. Sci. Rep. **71**, 547 (2016).
- [2] Y. Fukaya, A. Kawasuso, A. Ichimiya, and T. Hyodo, J. Phys. D **52**, 013002 (2019).
- [3] Y. Fukaya, in *Monatomic Two-Dimensional Layers*, edited by I. Matsuda (Elsevier, 2019), Micro and Nano Technologies, pp. 75 – 111.
- [4] R. Feidenhans'l, Surf. Sci. Rep. **10**, 105 (1989).
- [5] H. Tajiri, Jpn. J. Appl. Phys. **59**, 020503 (2020).
- [6] M. A. V. Hove, W. Moritz, H. Over, P. Rous, A. Wander, A. Barbieri, N. Materser, U. Starke, and G. A. Somorjai, Surf. Sci. Rep. **19**, 191 (1993).
- [7] K. Tanaka, T. Hoshi, I. Mochizuki, T. Hanada, A. Ichimiya, and T. Hyodo, Acta. Phys. Pol. A **137**, 188 (2020).
- [8] K. Tanaka, I. Mochizuki, T. Hanada, A. Ichimiya, T. Hyodo, and T. Hoshi, JJAP Conf. Series, in press; Preprint: <https://arxiv.org/abs/2002.12165/>.
- [9] T. Hoshi, D. Sakata, S. Oie, I. Mochizuki, S. Tanaka, T. Hyodo, and K. Hukushima, Comp. Phys. Commun. **271**, 108186 (2022).
- [10] J. A. Nelder and R. Mead, Comput J **7**, 308 (1965).
- [11] M. Wright, in *Numerical analysis*, edited by D. Griffiths and G. Watson (Addison-Wesley, 1996), pp. 191–208.
- [12] C. E. Rasmussen and C. K. I. Williams, *Gaussian Processes for Machine Learning (Adaptive Computation and Machine Learning)* (The MIT Press, 2005), ISBN 026218253X.
- [13] K. Hukushima and K. Nemoto, J. Phys. Soc. Jpn. **65**, 1604 (1996).
- [14] K. Hukushima and Y. Iba, AIP Conf. Proc. **690**, 1604 (2003).
- [15] L. Dalcín, R. Paz, and M. Storti, J. Parallel Distrib. Comput. **65**, 1108 (2005).
- [16] L. Dalcín, R. Paz, M. Storti, and J. D’Elía, J. Parallel Distrib. Comput. **68**, 655 (2008).
- [17] L. D. Dalcín, R. R. Paz, P. A. Kler, and A. Cosimo, Adv. Water Resour. **34**, 1124 (2011).
- [18] L. Dalcín and Y.-L. L. Fang, Comput. Sci. Eng. **23**, 47 (2021).
- [19] scipy, <https://scipy.org/>.
- [20] PHYSBO, <https://www.pasums.iissp.u-tokyo.ac.jp/physbo/>.
- [21] Y. Motoyama, R. Tamura, K. Yoshimi, K. Terayama, T. Ueno, and K. Tsuda, Comp. Phys. Commun. **278**, 108405 (2022).
- [22] R. M. Neal, Stat. Comput. **11**, 125 (2001).
- [23] M. Anada, Y. Nakanishi-Ohno, M. Okada, T. Kimura, and Y. Wakabayashi, J. Appl. Cryst. **50**, 1611 (2017).
- [24] K. Nagai, M. Anada, Y. Nakanishi-Ohno, M. Okada, and Y. Wakabayashi, J. Appl. Cryst. **53**, 387 (2020).
- [25] sim-trhepd-rheed, <https://github.com/sim-trhepd-rheed/>.
- [26] T. Hanada, H. Daimon, and S. Ino, Phys. Rev. B **51**, 13320 (1995).
- [27] T. Hanada, Y. Motoyama, K. Yoshimi, and T. Hoshi, Comp. Phys. Commun. **277**, 108371 (2022).
- [28] I. Mochizuki, H. Ariga, Y. Fukaya, K. Wada, M. Maekawa, A. Kawasuso, T. Shidara, K. Asakura, and T. Hyodo, Phys. Chem. Chem. Phys. **18**, 7085 (2016).
- [29] Y. Endo, Y. Fukaya, I. Mochizuki, A. Takayama, T. Hyodo, and S. Hasegawa, Carbon **157**, 857 (2020).
- [30] sxrdcalc, <https://github.com/sxrdcalc/>.
- [31] W. Voegeli, K. Akimoto, T. Aoyama, K. Sumitani, S. Nakatani, H. Tajiri, T. Takahashi, Y. Hisada, S. Mukainakano, X. Zhang, et al., Appl. Surf. Sci. **252**, 5259 (2006).
- [32] ANA-ROD, [https://www.esrf.fr/computing/scientific/joint\\_projects/ANA-ROD](https://www.esrf.fr/computing/scientific/joint_projects/ANA-ROD).
- [33] E. Vlieg, J. Appl. Cryst. **33**, 401 (2000).
- [34] CTR-structure, <https://github.com/yusuke-wakabayashi/CTR-structure>.
- [35] T. Hirahara, S. Ereemeev, T. Shirasawa, O. Yuma, T. Kubo, R. Nakanishi, R. Akiyama, A. Takayama, T. Hajiri, S. Ideta, et al., Nano Lett. **17**, 3493 (2017).
- [36] S. Y. Tong, Surf. Sci. **457**, L432 (2000), ISSN 0039-6028.
- [37] K. Wada, T. Shirasawa, I. Mochizuki, M. Fujinami, M. Maekawa, A. Kawasuso, T. Takahashi, and T. Hyodo, e-J. Surf. Sci. Nanotechnol. **16**, 313 (2018).
- [38] H. H. Rosenbrock, Comput. J. **3**, 175 (1960).
- [39] D. H. Ackley, *A connectionist machine for genetic hillclimbing* (Kluwer Academic Publishers, Boston, 1987).
- [40] D. Himmelblau, *Applied Nonlinear Programming* (McGraw-Hill, 1972).
- [41] H. Kohashi, H. Iwamoto, T. Fukaya, Y. Yamamoto, and T. Hoshi, JSIAM Letters **14**, 13 (2022).
- [42] TOML, <https://toml.io/en/>.
- [43] tomli, <https://pypi.org/project/tomli/>.
- [44] numpy, <https://numpy.org/>.
- [45] Y. Motoyama, K. Yoshimi, T. Kato, and S. Todo (2022), URL <https://arxiv.org/abs/2205.01991>.
- [46] A. Ichimiya, Surf. Sci. Lett. **192**, L893 (1987).
- [47] T. Shirasawa, S. Mizuno, and H. Tochiara, Surf. Sci. **600**, 815 (2006).
- [48] Quantum Espresso, <https://www.quantum-espresso.org>.

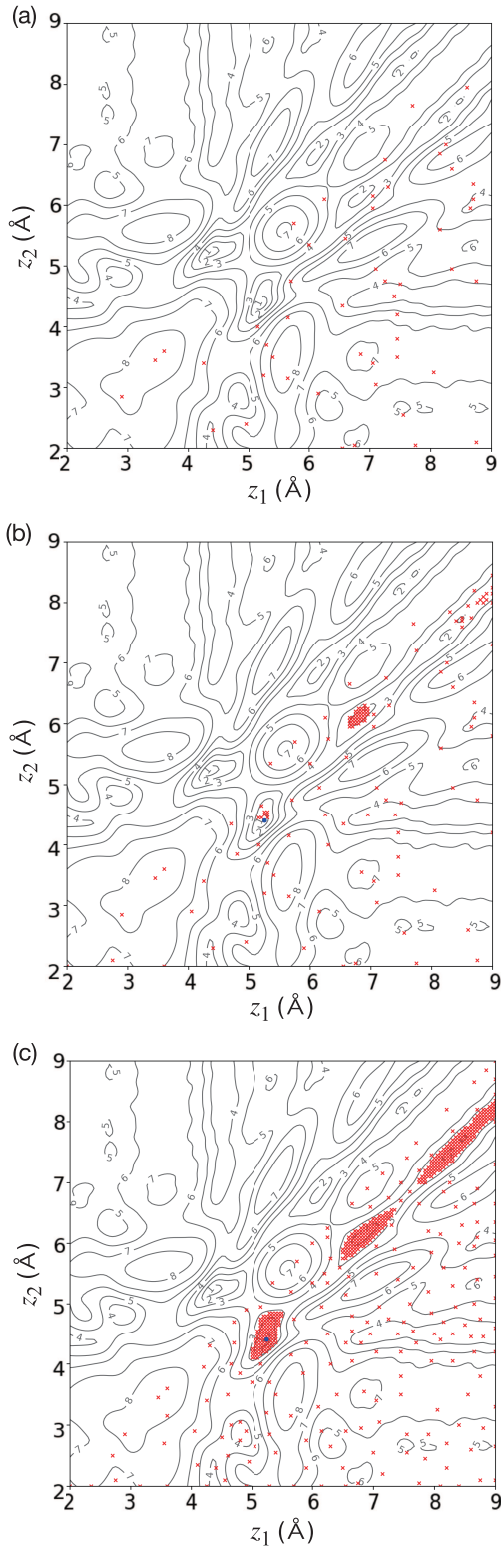


Figure 7: Search points  $\{(z_1^{(j)}, z_2^{(j)})\}_j$  in BO analysis of TRHEPD data for Ge(001)-c(4 × 2) surface with (a)  $j = 0, \dots, 49$ , (b)  $j = 0, \dots, 127$ , and (c)  $j = 0, \dots, 449$ . The grid minimum point  $(z_1, z_2) = (5.25\text{\AA}, 4.4\text{\AA})$  is indicated by a filled circle, and the other search points are indicated by crosses. The contour of  $F$  is also plotted as a guide for the eye.

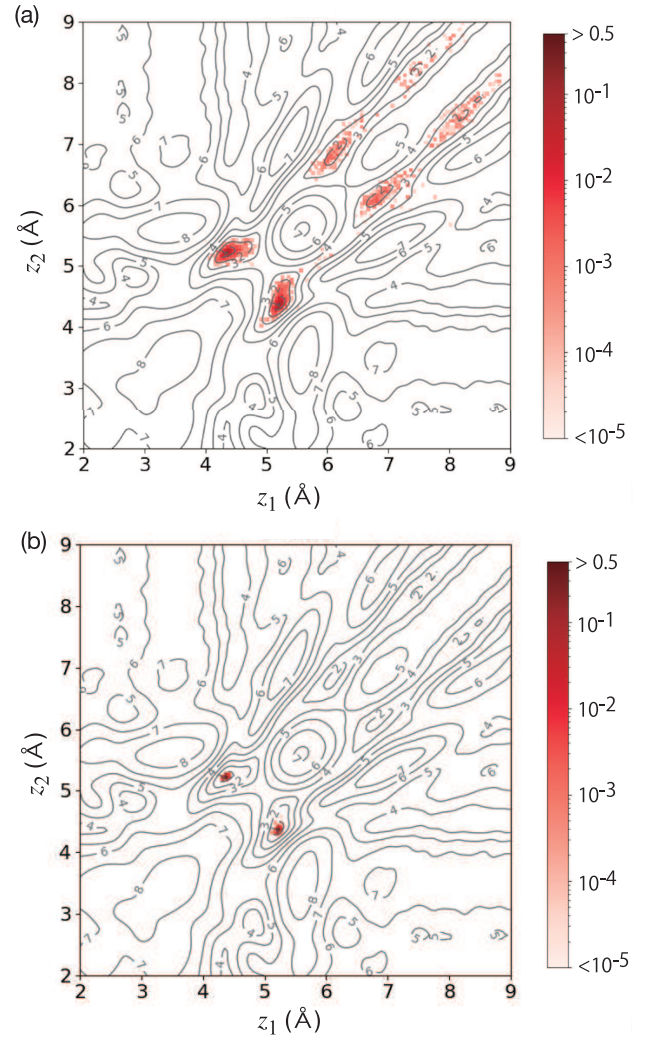


Figure 8: Replica exchange Monte Carlo (REMC) analysis of TRHEPD data for Ge(001)-c(4 × 2) surface. The histograms of the posterior probability density  $\pi(z_1, z_2|D; \tau)$  are drawn for temperature parameters of (a)  $\tau = 0.0029$  and (b)  $\tau = 0.001$ . The contour of  $F$  is also plotted as a guide for the eye.

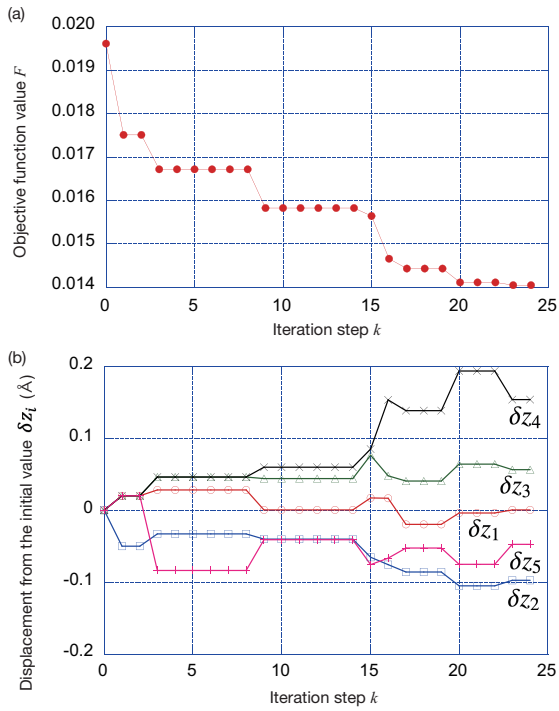


Figure 9: Nelder-Mead optimization analysis of the experimental TRHEPD data for Ge(001)-c( $4 \times 2$ ) surface. (a) The objective function  $F = F(z_1^{(k)}, z_2^{(k)}, z_3^{(k)}, z_4^{(k)}, z_5^{(k)})$  and (b) the deviations from the initial values  $\delta z_i^{(k)} = z_i^{(k)} - z_i^{(0)}$  ( $i = 1, 2, 5$ ) are plotted as functions of the iteration step  $k (= 0, 1, 2, \dots)$ .

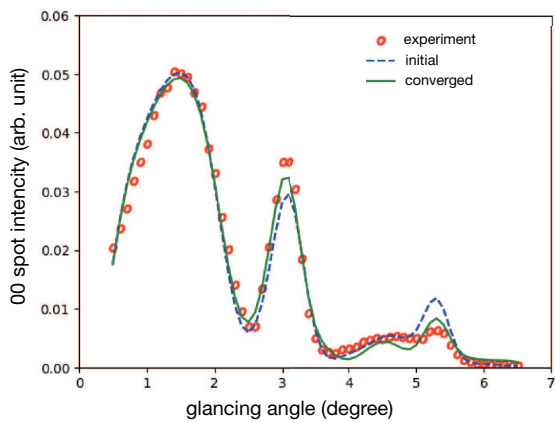


Figure 10: Comparison between the experimental rocking curve (open circles), the calculated ones for the initial (dashed line) and converged (solid line) structures in the Nelder-Mead optimization analysis of the experimental TRHEPD data for Ge(001)-c( $4 \times 2$ ) surface.